






Article

Environmental-Friendly Adsorbent Composite Based on Hydroxyapatite/Hydroxypropyl Methyl-Cellulose for Removal of Cationic Dyes from an Aqueous Solution

Noureddine Akartasse ^{1,*}, Khalil Azzaoui ¹, Elmiloud Mejdoubi ¹, Belkheir Hammouti ^{1,2},
Lhaj Lahcen Elansari ¹, Mohamed Abou-salama ³, Mohamed Aaddouz ¹, Rachid Sabbahi ^{4,5},
Larbi Rhazi ^{6,*} and Mohamed Sijaj ^{7,*}

¹ Laboratory of Applied Chemistry and Environment, Department of Chemistry, Faculty of Sciences, Mohammed 1st University, P.O. Box 717, Oujda 60000, Morocco; k.azzaoui@yahoo.com (K.A.); ee.mejdoubi@gmail.com (E.M.); hammoutib@gmail.com (B.H.); elansarihassan@yahoo.fr (L.L.E.); m.aaddouz@ump.ac.ma (M.A.)

² CREHEIO, Ecole des Hautes Etudes d'Ingénierie, Oujda 60000, Morocco

³ Laboratory of Molecular Chemistry, Department of Chemistry, Materials and Environment, Faculty Multidisciplinary Nador, University Mohammed Premier, B.P. 300, Selouane, Nador 62700, Morocco; m.abousalama@ump.ac.ma

⁴ Higher School of Technology, University of Ibn Zohr, Quartier 25 Mars, P.O. Box 3007, Laayoune 70000, Morocco; r.sabbahi@uiz.ac.ma

⁵ Laboratory of Plant Biotechnology, Faculty of Sciences, University of Ibn Zohr, Hay Dakhla, P.O. Box 8106, Agadir 80000, Morocco

⁶ Institut Polytechnique UniLaSalle, Transformations & Agro-Resources Research Unit (ULR7519), 19 rue Pierre Waguet, BP 30313, 60026 Beauvais, France

⁷ Department of Chemistry and Biochemistry, Université Du Québec à Montréal, Montréal, QC H3C 3P8, Canada

* Correspondence: noureakar@yahoo.fr (N.A.); larbi.rhazi@unilasalle.fr (L.R.); mohamed.sijaj@uqam.ca (M.S.); Tel.: +33-344-067-552 (L.R.); +1-514-9873000 #1921 (M.S.)



Citation: Akartasse, N.; Azzaoui, K.; Mejdoubi, E.; Hammouti, B.; Elansari, L.L.; Abou-salama, M.; Aaddouz, M.; Sabbahi, R.; Rhazi, L.; Sijaj, M. Environmental-Friendly Adsorbent Composite Based on Hydroxyapatite/Hydroxypropyl Methyl-Cellulose for Removal of Cationic Dyes from an Aqueous Solution. *Polymers* **2022**, *14*, 2147. <https://doi.org/10.3390/polym14112147>

Academic Editors:
Przemysław Pączkowski
and Beom Soo Kim

Received: 20 April 2022

Accepted: 19 May 2022

Published: 25 May 2022

Publisher's Note: MDPI stays neutral with regard to jurisdictional claims in published maps and institutional affiliations.



Copyright: © 2022 by the authors. Licensee MDPI, Basel, Switzerland. This article is an open access article distributed under the terms and conditions of the Creative Commons Attribution (CC BY) license (<https://creativecommons.org/licenses/by/4.0/>).

Abstract: The aim of this study is to develop a new, efficient, and inexpensive natural-based adsorbent with high efficacy for the cationic dye methylene blue (MB). A natural-based nanocomposite based on hydroxyapatite (HAp) and hydroxypropyl methylcellulose (HPMC) was selected for this purpose. It was synthesized by the dissolution/precipitation method. A film with a homogeneous and smooth surface composed of nanoparticles was prepared from the nanocomposite. HPMC and HAp biopolymers were selected due to their compatibility, biodegradability, and non-toxicity. Total reflectance infrared spectroscopy (ATR-FTIR), scanning electron microscopy (SEM), and calorimetric/thermal gravimetric (DSC/TGA) analysis results revealed the existence of strong physical interaction between the composite components. Scanning electron microscopy (SEM) observations show a composite sheet with a homogenous and smooth surface, indicating excellent compatibility between HPMC and HAp in the composite. The nanocomposite was evaluated as an adsorbent for organic dyes in an aqueous solution. The effects of solution pH, initial MB concentration, composite concentration, and adsorption time on the adsorption efficiency were evaluated. The highest adsorption rate was seen as 52.0 mg of MB/g composite. The adsorption rate reached equilibrium in about 20 min. Fitting of the adsorption data to the Langmuir and Freundlich adsorption models was investigated. Results showed that the adsorption process follows the Langmuir isotherm model. The kinetic study results revealed that the adsorption process was pseudo-second-order. The herein composite is an excellent alternative for use as contemporary industrial-scale adsorbents.

Keywords: nanocomposite; hydroxypropyl methylcellulose; hydroxyapatite; methylene blue; adsorption

1. Introduction

Organic dyes from factories such as textiles, cosmetics, gasoline, printing, and plastics generate toxic substances that cause a significant pollution issue when discarded into the waste stream without any further treatment [1]. This is considered an emergent issue since such industries are not paying attention to the treatment of dyes before discharge to the environment. This behavior might have a severe impact on the health of humans, animals, and living organisms [2]. The biological degradation of the generated dyes is not always possible [2] since they are known to have a complex aromatic molecular structure that makes them very stable and display a xenobiotic behavior [3].

So, removal of these pollutants by other means becomes a high priority. Several methods are known to be useful in this regard, notably coagulation-precipitation by flocculation [4], membrane cake filtration [5], and electrocoagulation [6]. From these techniques, the adsorption process has been proven to be a very reliable and cost-effective process for the removal of pollutants [7].

Methylene blue is among the organic dyes present in the waste stream generated from the coloring industry processing textiles, paper, leather, food, and cosmetics [8]. In addition, methylene blue (MB) is a commonly used dye as a disinfectant in medicine, pharmaceuticals, pesticide production, varnish, and lacquer manufacturing [9]. It is a cationic dye with a chemical structure presented in Figure 1. It is known to cause various undesirable damage to living creatures, including permanent eye burns, breathing disorders, heart rate increases, tissue necrosis, nausea, vomiting, mental confusion, and painful micturition [10]. For this reason, the dye methylene blue was chosen as a cation dye model in this study. Among the conventional methods for removing methylene blue and other dyes from wastewater, adsorption is the most efficient. The adsorption method is the most widely used since it is simple, can be performed at low cost, and offers good efficiency. However, the available technological means to improve the adsorption process are adverse. Adsorption is a surface phenomenon based on the interaction between adsorbents in the solid phase and adsorbates in the liquid or gas phase [10–13]. The efficiency, capacity, and reusability of the adsorbent material depend on the functional groups on the adsorbent surface. In this case, the adsorption efficiency is controlled by the type and the strength of the interaction between the functional groups of the adsorbent and the adsorbate. So, the adsorbent selection is a crucial factor in this process [14]. Natural-based materials [15] and agricultural industrial by-products [16] are examples of low-cost adsorbents with functionalities that have a high affinity for MB.

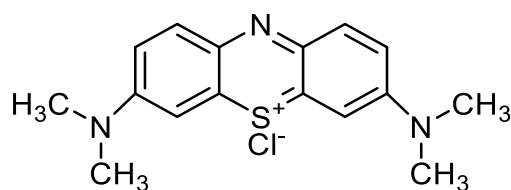


Figure 1. Chemical structure of methylene blue $C_{16}H_{18}ClN_3S \times H_2O$.

Among these, clay is widely used as an adsorbent because it has advantages such as low cost, abundant availability, non-toxicity, and large surface area. Clay minerals that harden when dried are flexible by nature. These are fine-grained minerals that are naturally found on the soil surface [17,18]. Natural clay has limited applications due to its low adsorption capacity. Yet, its chemical surface yields the possibility of being modified and/or functionalized [19]. Marl, known as cement clay, is a low-cost clay composed of 50–70% limestone and 30–50% clay. In the cement industry, it is the only natural raw material where clay and limestone are found together.

In recent years, polymeric fibers have been used as adsorbents for the removal of dyes from aqueous media due to their relatively low cost, high specific surface area, and fast adsorption kinetics. For example, IDA-GMA-g-PET fibers have been exploited for

the removal of the dyes Malachite Green (MG) and Rhodamine B (RB) [20]. MB has been removed using plasma activated acrylic acid grafted polypropylene (AA-PP) [21] and β -cyclodextrin graft modified polypropylene (PP) [22]. Graphene oxide (GO)-containing hydrogels were also investigated due to their high surface area and ability to adsorb a large amount of water and water-soluble molecules [23]. However, cellulose is the most abundant material in nature. Its derivatives have been widely used in water treatment [24]. Cellulosic fibers are considered low-cost biosorbents and ideal functional substrates for the removal of organic and inorganic pollutants [25]. They can be easily modified by grafting various functional groups onto the surface-active hydroxyl moieties [26]. Moreover, modified cellulose could be prepared as a functional component of a hybrid composite by incorporation with other materials [27–30].

Activated carbon or material-based activated carbon was the most used adsorbent because of its high capacity to adsorb organic matter [23,31,32].

The use of Hap-based composites as adsorbents has raised great interest because of their efficiency and accessible cost [33–37].

Calcium phosphate materials, such as Haps, are unique inorganic compounds and the main mineral constituent of teeth, bones, and phosphate mineral materials. Because of its high capacity to remove divalent heavy metal ions, synthetic hydroxyapatite has been used to remove heavy metals such as Pb, Cr, Zn, Cu, Cd, Co, V, Ni, and Sb from water [38–45].

Recently, the synthesis of this type of phosphocalcic material has been widely studied in the literature for many applications [29,46,47]. In this context, the modification of the surface of hydroxyapatite to form composites with various organic and inorganic substances should give new functions to this material [48]. In fact, the interaction between hydroxyapatite calcium and biopolymers has been the subject of numerous studies, including HPMC, carboxymethylcellulose [49], collagen [47–49], polycaprolactone [50], sodium caseinate [51], Agar-Agar [52], chitosan [53], alginate [54], and gelatin [55,56]. These composite materials have been developed for a large variety of applications: bone substitution [57], tissue repair engineering [58], and biomedical and environmental fields [59].

The HPMC is a cellulose derivative in which part of the (OH) groups are replaced by a methyl and hydroxypropyl group Figure 2. These changes increased its solubility in an aqueous solution.

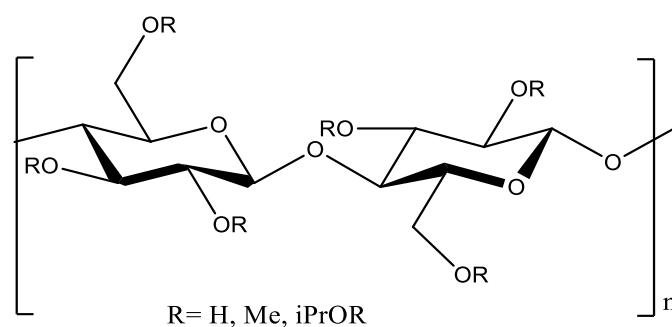


Figure 2. Structure of (HPMC) [60].

HPMC is an odorless and flavorless additive unmetabolized by humans, resistant to enzymes, and stable in pH between 2 and 13.

The objective of this study is to develop a new, efficient, and inexpensive adsorbent composite capable of interacting with the cationic dye MB. The dissolution/precipitation process was used for making the composite [61], which will allow the elaboration of nano-composites based on hydroxyapatite $[Ca_{10}(PO_4)_6(OH)_2]$ and HPMC. Subsequently, several composites with various ratios of HAp/HPMC were synthesized. Then, the ability of HAp/HPMC composites to remove MB ions from aqueous solutions under various conditions was investigated.

2. Materials and Methods

2.1. Materials

The reagents and solvents used in this work were acquired from Sigma Aldrich (Burlington, MA, USA) and used without further purification. Reagents include: calcium nitrate tetrahydrate ($\text{Ca}(\text{NO}_3)_2 \cdot 4\text{H}_2\text{O}$, 99%), diammonium hydrogen phosphate ($(\text{NH}_4)_2 \cdot \text{HPO}_4$, 99%), methylene blue $\text{C}_{16}\text{H}_{18}\text{ClN}_3\text{S} \cdot \text{H}_2\text{O}$ (molecular weight 319.85 g/mol), hydroxypropyl methylcellulose (molecular weight 86 kDa), ammonia solution NH_4OH (Supelco), and perchloric acid HClO_4 , 70%.

2.2. Hydroxyapatite/Hydroxypropylmethylcellulose HAp/HPMC Composites

Hydroxypropyl methylcellulose is a hydrophilic cellulosic derivative soluble in cold aqueous solutions. The HAp/HPMC/ H_2O solution was prepared using the dissolution/reprecipitation process [62]. An amount of 1.5 g of hydroxypropyl methylcellulose was immersed into 150 mL of distilled water under continuous stirring at room temperature. This preparation was labeled as solution A. Hydroxyapatite solution was prepared by mixing 0.5 g of hydroxyapatite with 50 mL distilled water containing 0.5 mL HClO_4 ($d = 1.67 \text{ g/cm}^3$) under continuous stirring at room temperature. The last solution was identified as solution B. Solution B was poured dropwise to solution A. The produced mixtures were brought to an adequate basic pH value by adding NH_4OH . The mixtures were stirred for 2 h at 30 °C to obtain translucent colloidal suspensions. The translucent solutions obtained were poured into Petri dishes and left to dry at room temperature for 3 days.

2.3. Methods

In this study, the Infrared spectra were recorded using a Nicolet 6700 Fourier Transform Infrared (FT-IR) spectrometer supplied with the Smart SplitPea micro-ATR accessory (Shimadzu Scientific, Duisburg, Germany). The FT-IR spectra were collected at a resolution of 4 cm^{-1} , covering the spectral range of $600\text{--}4000 \text{ cm}^{-1}$ and 64 scans.

The scanning electron microscopy (SEM) analysis was performed using a SU 8020, 3.0 KV SE (Hitachi High-Technologies Corporation, Tokyo, Japan). Before the analysis, all specimens were frozen using liquid nitrogen, fractured, mounted, coated with gold/palladium, and observed using an applied bias of 10 kV.

The standard thermogravimetric analysis was performed on the composites using the TGA Q500 and Q50 TA instrument (Shimadzu, Germany) at a temperature range from 20–900 °C and a heating rate of 10 °C/min.

X-ray Diffraction (XRD) model (XPRT-PRO, PW3050/60) (LabXRD-6100 Shimadzu, Germany) was used to analyze the powder diffraction at room temperature using a Diffractometer with $\text{CuK}\alpha$ radiation (1.5418 \AA) in the range of $20^\circ \leq 2\theta \leq 80^\circ$ using a sweep rate of $2^\circ/\text{min}$.

2.4. Surface Characterization

The surface analysis was performed using several instruments. The Atomic Force Microscopy (AFM) was used to study the cellulose blend surface morphology changes at 303 K. The measurements were performed utilizing a VEECO CPII atomic force microscope model (MPP-11123, Germany) at the cantilever's resonance frequency between 335–363 kHz with a variable spring constant (k) of 20–80 N/m. During the X-ray photoelectron spectroscopy (XPS) experiment, the spectra were recorded using a Physical Electronic (PHI 5700 spectrometer, Germany) using a hemispherical multichannel detector with a constant pass energy mode at 30.1 eV, involving a 730 μm diameter analysis area. The data were analyzed using PHI ACCESS ESCA-V6.0F software. In order to find the binding energy values, a carbon C_{1s} signal with a value of 284.6 eV was used for the characterization of the rest of the binding energies [63]. During the analysis, Shirley-type background and Gauss-Lorentz curves were involved.

2.5. Adsorption

The cationic dye MB was selected for this study. The adsorption process was carried out using the batch method [64,65]. In this method, a 10.0 mg sample of the adsorbent was used per 10 mL of MB solution with various concentrations ranging from 40 to 300 mg/L. The adsorption was carried out at 25 °C at a stirring speed of 250 rpm. The effect of pH and the adsorption time on the adsorption efficiency were evaluated. The pH was adjusted by the addition of either HNO₃ or NH₄OH [65–67].

Samples of the reaction mixture were taken at regular time intervals to monitor the residual MB concentration. The samples taken were filtered and analyzed using a spectro UV–visible spectrophotometer type (MACY UV-1100, Germany) at a wavelength of 665 nm corresponding to the maximum MB adsorption (λ_{\max}). The residual concentration of the dye solution was calculated from the external standard curve.

The change in the concentration of MB was monitored by UV spectrophotometry. The nanocomposites' adsorption capacity for MB was calculated as shown in Equations (1) and (2) [23]:

$$R (\%) = \frac{C_0 - C_e}{C_0} 100 \quad (1)$$

$$Q_e = \frac{C_0 - C_e}{m} V \quad (2)$$

C_0 and C_e are the initial and equilibrium concentrations (ppm) of cadmium in solution, respectively. Q_e (ppm) is the equilibrium adsorption capacity, m is the weight of the adsorbent (mg), R the capacity for adsorption, and V is the volume of the solution (L).

2.6. Zero-Point Contaminated pH (pHpzc)

The zero-charge point, pHpzc, is the pH at which the average surface charge is zero [54], but this does not mean that there are no positive and negative charges; it means that the number of charges in the two categories are identical ($[\text{MO}^-] = [\text{MOH}_2^+]$). This parameter is very important in adsorption phenomena, especially when electrostatic forces are involved in the mechanisms.

A quick and easy way to determine pHpzc is to use the pH drift method (potentiometric titrations). In this method, several flasks (100 mL), each containing a 60 mg sample of the composite and 20.0 mL of 0.1 M KNO₃. The initial pH of each solution was adjusted in the range between 4 and 11 by adding a small volume of NaOH or HCl solutions (0.1 M) and measured on pH/ion meter. The suspensions were kept stirred at room temperature for 6 h, and the final pH was then determined. The pHpzc is the point at which the final pH versus initial pH curve intersects the $\text{pH}_{\text{final}} = f(\text{pH}_{\text{initial}})$ regression line [68,69].

2.7. Adsorption Analysis

Langmuir (Equation (3)) and Freundlich isotherm (Equation (5)) models were applied to investigate the adsorption equilibrium between MB solution and the HAp/HPMC composite polymer [51]. Both models were used to assess the MB dispersion on the surface of the HAp/HPMC composites once equilibrium was reached under constant temperature.

The factor dictating the type of isotherm model is the correlation coefficient, R^2 [51].

$$\frac{C_e}{Q_e} = \frac{1}{q_{\max}} C_e + \frac{1}{q_{\max} K_L} \quad (3)$$

where C_e represents the equilibrium concentration of the adsorbate (mg/L), Q_e is the amount of the adsorbate adsorbed per unit mass of HAp/HPMC composite at equilibrium (mg/g), q_{\max} is the adsorption capacity equilibrium (mg/g), and K_L is the Langmuir affinity constant (L/mg).

In the Langmuir isotherm model, the R_L ratio is sometimes referred to as a dimensionless quantity indicating whether sorption is favorable or not.

$$R_L = \frac{1}{1 + K_L C_0} \quad (4)$$

where C_0 is the initial adsorbate concentration. If the value of R_L is higher than 1, the adsorption is unfavorable. However, when the R_L value is between 1 and 0, the adsorption is favorable. When $R_L = 1$, adsorption is linear.

The Freundlich isotherm is an empirical formula used for low concentrations and is presented as [51]:

$$\ln(Q_e) = \ln K_F + \frac{1}{n} \ln C_e \quad (5)$$

where K_F is the Freundlich constant that deals with adsorption capacity (mg/g) and n is the heterogeneity coefficient which describes how favorable the adsorption process is (g/L).

3. Results

The current study presents a natural-based composite for the removal of methylene blue from wastewater. The composite was synthesized by dissolution/reprecipitation process using two natural-based materials, hydroxyapatite and hydroxypropyl methylcellulose. The composite was deposited as a membrane. The membrane showed excellent optical properties. Macroscopically, it is a thin and transparent film (Figure 3a,b). The film shows excellent dispersion of the apatite grains (inorganic phase) in the organic matrix.

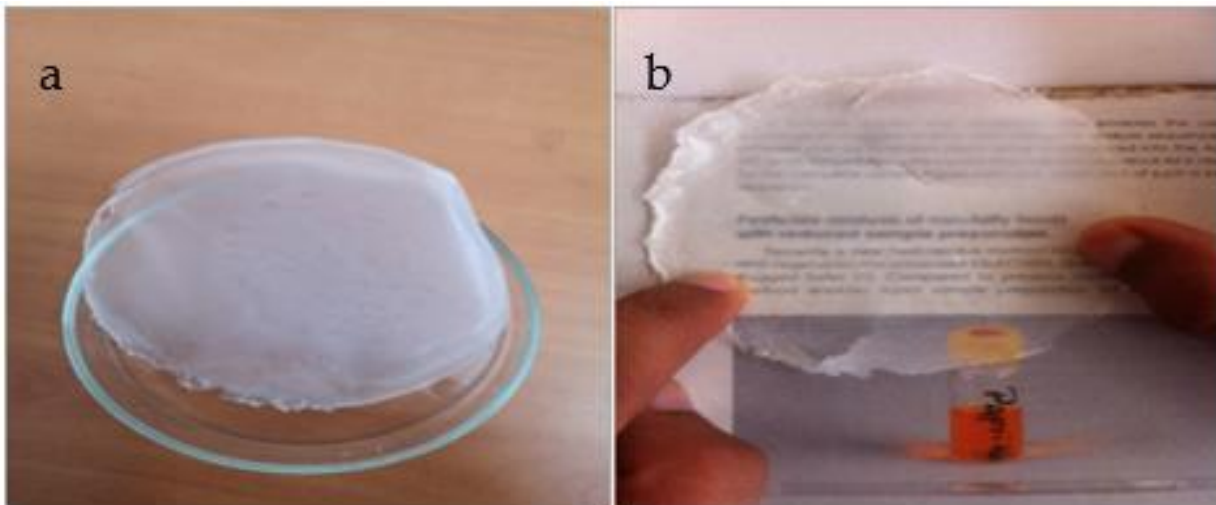


Figure 3. Image of the HAp/HPMC membrane. (a) thin and homogenous film and (b) transparent film.

The FT-IR spectra of HAp, HPMC and a composite of 30 wt.% HAp and 70 wt.% HPMC are overlaid in Figure 4. The spectrum of HPMC shows a band at about 3460 cm^{-1} corresponding to the stretching vibrations of the O-H bond. The Infrared spectrum also shows a band at 2800 cm^{-1} due to the stretching vibration of C-H bonds concerning the methyl and hydroxypropyl groups of HPMC. The band at 1643 cm^{-1} corresponds to the vibrations of the cyclic C-O bond [70]. The band at 1093 cm^{-1} corresponds to the elongation vibration of the glycosidic linkage C-O-C [70,71].

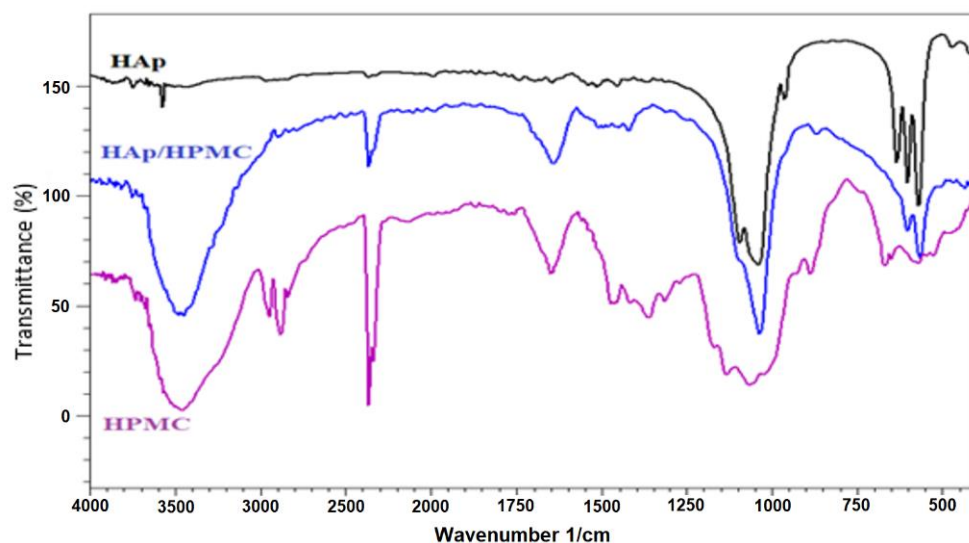


Figure 4. FT-IR spectra of HAp alone, HAp/HPMC and HPMC.

The FT-IR spectrum of HAp shows bands at 1090, 1033, 962, 603, and 561 cm^{-1} , which could be attributed to the PO_4^{3-} clusters of the apatite network. The composite shows a spectrum with different peaks that have different HAp intensity, and wavenumber compared to those of the starting material, which indicates the presence of strong interactions between the composite components.

The HAp/HPMC composite was also subjected to analysis by solid-state ^{13}C NMR to get a better picture of the strength of the interaction between the composite components compared to HPMC in Figure 5. The HPMC spectrum peaks are assigned as follows: C1' (101–104 ppm), C2'-5' (72–85 ppm), and C6' (58–64 ppm). Those from HPMC were assigned to C1* (104 ppm), C2* (97 ppm), C3*-5*, 2-6* (70–90 ppm), C6.c (67 ppm), and Ca (20 ppm).

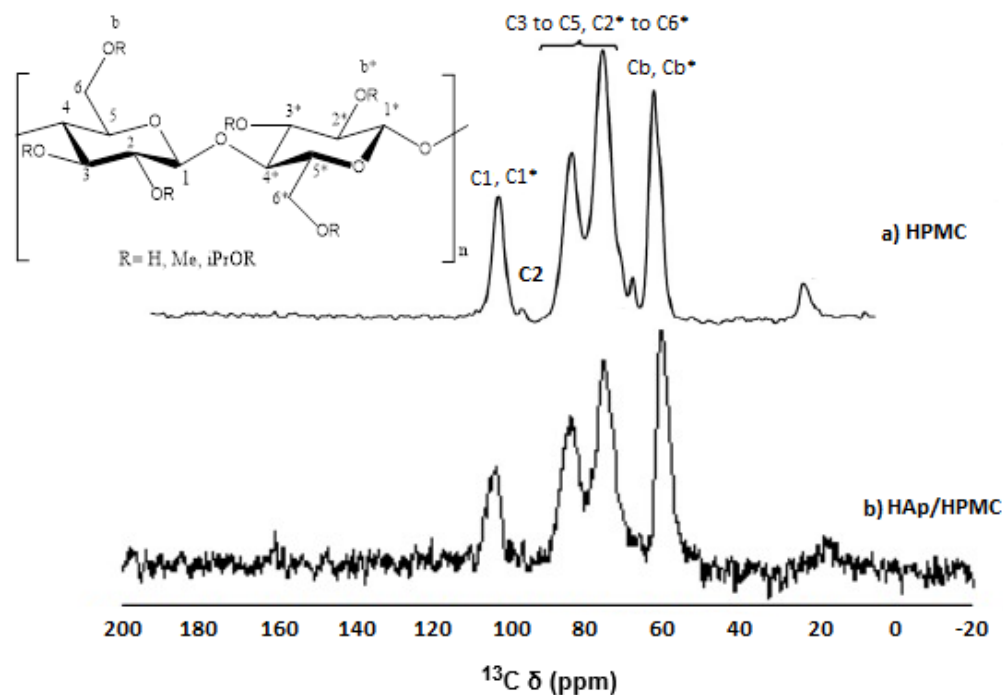


Figure 5. ^{13}C CP-MAS solid-state NMR spectra (a) HPMC (b) HAp/HPMC.

In the spectrum of HAp/HPMC grafted film, the resonance peak due to C-band Cb* (methoxy groups) of HPMC showed a shoulder at ~59 ppm, which may be due to C6 of HPMC; we noticed a movement toward 57 ppm of HAp/HPMC composite.

In our study and analysis, the resonance peak, which is related to the methoxy carbons of HPMC, was labeled into three Voigt components, one at 59.30 ppm (Cb) and the other two at 61.42 ppm (Cb*). In the case of the spectrum of HAp/HPMC grafted composite, the identified Voigt component, which refers to C band Cb*, was shifted to 59.63 ppm and 61.52 ppm involving an increase in the peak area of the latter. This is probably due to the interference of the peaks corresponding to the C6 of grafted HAp/HPMC.

3.1. X-ray Diffraction

The prepared composites were characterized by X-ray diffraction. The XRD diffractograms of the HAp/HPMC composite, with weight ratios of 30 to 70, are shown in Figure 6. The composite shows that the apatitic structure is retained. The phenolphthalein test performed just after calcination of the composites at 900 °C showed the absence of the pink color (negative), which indicates a total absence of calcium oxide. The obtained Ca/P atomic ratio was less or equal to the stoichiometric hydroxyapatite (1.67) [72].

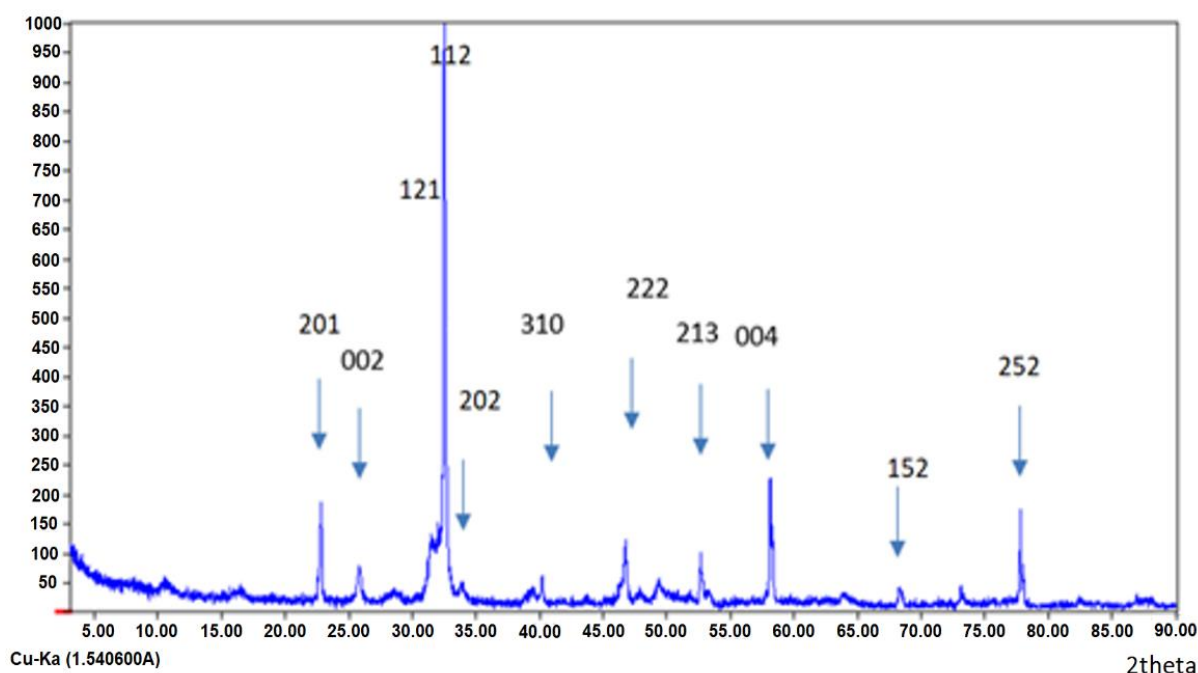


Figure 6. XRD diffractogram of the HAp/HPMC 30/70 composite.

The width at mid-height of the index lines (002) and (310) was used to determine the average crystallite size using Scherrer's formula [60–65]. The dimensions of the crystallites in the directions perpendicular to the (002) or (310) planes are given in Table 1. According to the obtained results, the dimensions of the nanoparticles evolve and are inversely proportional to the ratio of HPMC polymer to hydroxyapatite. So, the higher the ratio of HPMC polymer to mineral phase, the more space the apatite particles have to be deposited separately. The particle size was also calculated using Scherrer's formula (6) shown below [73–79].

$$D_p = \frac{0.94 \lambda}{\beta \cos \theta} \quad (6)$$

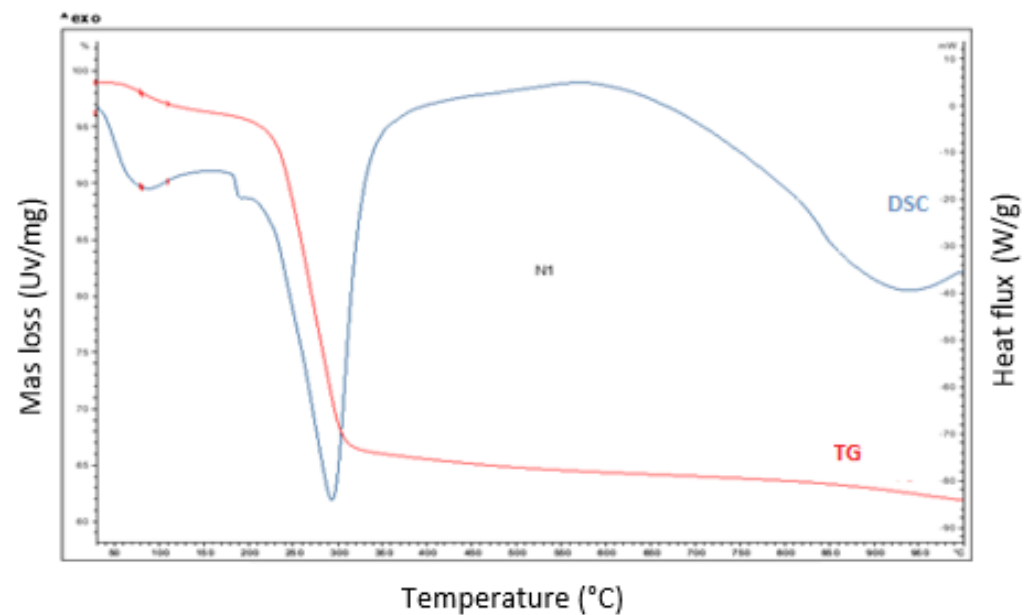
where 0.94 stands for a geometrical factor that depends on crystallite apparent radius of gyration from the perspective of reflections with Bragg angle θ for X-rays of wavelength λ .

Table 1. Average size of apatitic nanoparticles according to Scherrer's formula.

Compounds	$\lambda(\text{\AA})$	Planes hkl	D (nm)	D_{mean} (nm)
Pure HAp	1.5406	002 310	63 63	63
HAp/HPMC 30/70	1.5406	002 310	50 45	47
HAp/HPMC 20/80	1.5406	002 310	23 23	23

3.2. Thermal Analysis of HAp/HPMC Composite

The TGA curve of the HAp/HPMC (30/70) composite is shown in Figure 7. The curve shows two mass-loss events. The first is recorded between 50 and 100 °C, which corresponds to the loss of water. The second mass loss between 200 and 350 °C is attributed to the decomposition of the organic matter represented by HPMC. The two mass losses were confirmed by DSC as two endothermic peaks at 98 °C and 350 °C. The DSC reveals an endothermic transformation around 940 °C due to the partial decomposition of non-stoichiometric hydroxyapatite.

**Figure 7.** DSC/TGA curves of the HAp/HPMC composite.

3.3. Scanning Electron Microscopy

Scanning electron microscopy images of the HAp/HPMC composite (70/30) are shown in Figure 8. The images show a homogenous dispersion of hydroxyapatite particles in the polymer matrix with a nano size. The surface of the sample was irregular in shape and exhibited a rough morphology and agglomerated surface or in the form of a nano to micro-sized lump.

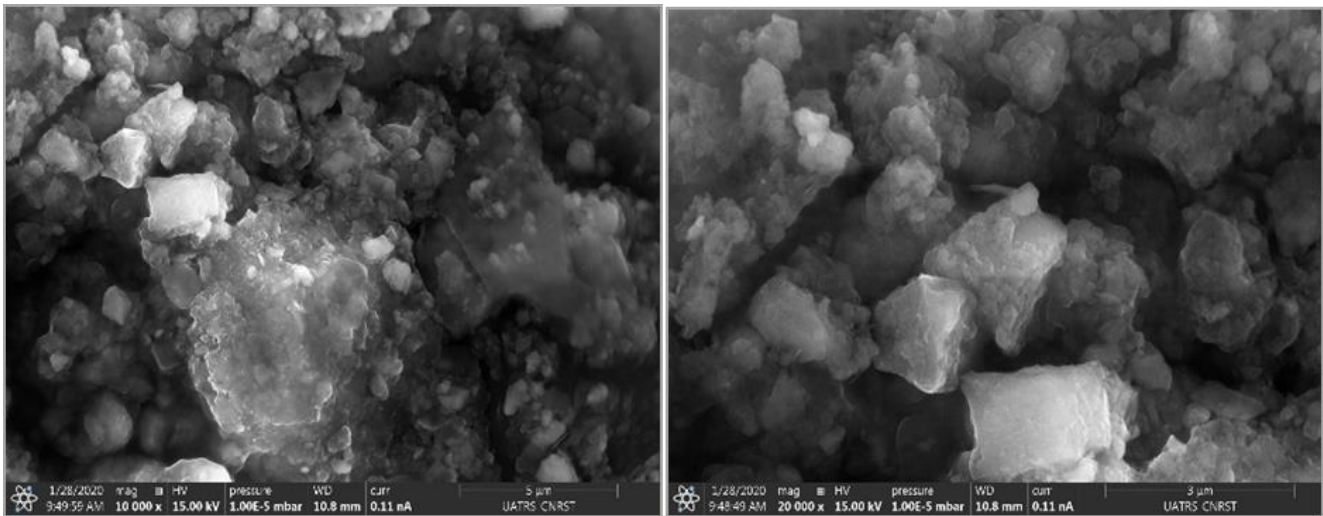


Figure 8. Scanning electron microscopy images of the HAp/HPMC composite (70/30).

3.4. Chemical Composition of the Composite

The main chemical elements of HAp/HPMC and their percentages are summarized in Table 2.

Table 2. Contents of the main elements in the chemical composition of the raw materials used in this study (by XRF method).

Element	wt (%)	Est.Error
Ca	28.82	0.23
Cl	13.47	0.17
P	16.83	0.16

XPS analysis was carried out on the HAp/HPMC composite (70/30) in order to obtain information about the Ca/P ration. This technique would be a good way to assess which termination (rich in calcium or rich in phosphate) is closest to the reality of the composite. It will simply be specified that the peaks used to obtain the Ca/P ratios are those relating to the 2p orbitals of calcium and phosphorus. Figure 9 shows that in favorable conditions for preparing the composite based on hydroxyapatite, the Ca/P ratio is lower than those obtained by chemical analysis; the surface is, therefore, less rich in calcium than the whole sample. This phenomenon was also observed by Tanaka, who deduced that the Ca atoms on the surface area were covered by an excess of phosphate ions [77]. It is possible to conclude that this difference between core and surface composition is quite specific to HAp.

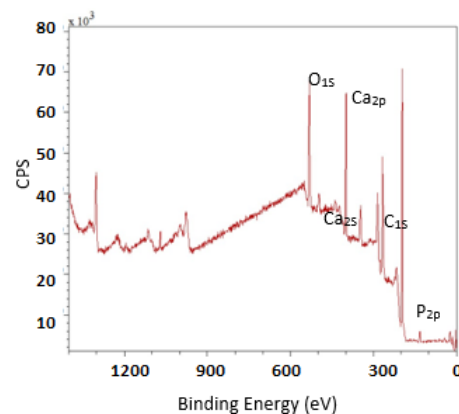


Figure 9. XPS spectra of the composite based on HAp/HPMC.

3.5. Adsorption of Methylene Blue on the Synthesized HAp/HPMC Composites

In this work, we are interested in using the prepared HAp/HPMC composite as an adsorbent of methylene blue colorant and determining the optimum adsorption conditions and composite component ratios.

3.6. Determination of the Zero-Load Point of HAp/HPMC Composite

The potentiometric titration method was performed in order to consider if BM at the surface of HAp/HPMC composite changed adsorbent surface charge by determination of the point of zero charge. The evolution of pH as a function of initial pH is shown in Figure 10. The first part of the curve, between the initial pH at 4 or 5, shows that the final pH of the solution increases as the initial pH increases. This is explained by the fact that the H^+ ions introduced into the solution are consumed by the surface of the material. Between initial pH 6 and initial pH 8 the curve becomes parallel to the x -axis (i.e., the final pH of the solution is stable). Indeed, all H^+ ions introduced in the solution are consumed by the surface of the material until saturation of the sites; then, there is a decrease in the final pH due to the consumption of OH^- ions via the deprotonation of the existing sites on the surface of the composite material.

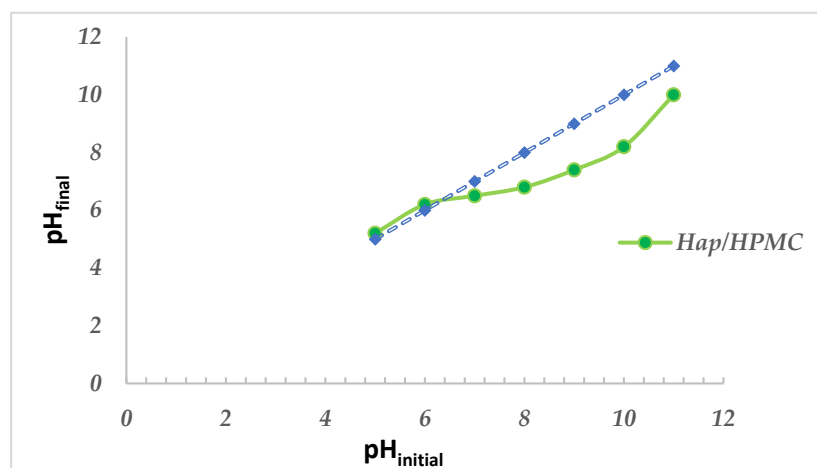


Figure 10. Determination of the pH_{pzc} of the composite material HAp/HPMC 60/40.

When the pH value is higher than pH_{pzc} , the surface of the solid is negatively contaminated, which favors the adsorption of cationic species. Meanwhile, when the pH values $< pH_{pzc}$, the surface is positively contaminated, favoring the adsorption of anionic species. The pH_{pzc} of the HAp/HPMC (60/40) composite is 6.4.

The results obtained show that the contamination developed on the surface of the composite material depends on the pH value.

Figure 11 shows the variation of the surface charge of HAp/HPMC composite as a function of pH.

The pH has a very important role in the adsorption phenomenon, as it can influence both the structure of the adsorbent and the adsorbate; it also might affect the adsorption mechanism. The study of the influence of pH on the adsorption of MB by the HAp/HPMC composite powder was performed using an initial MB concentration of 53.5 mg/L and a pH ranging from 6 to 12. The evolution of the amount of MB adsorbed as a function of pH is shown in Figure 12. The other variables, such as temperature, time, adsorbate mass, and the mixing speed, were kept constant at 25 °C, 30 min, 20 mg, and 250 rpm, respectively.

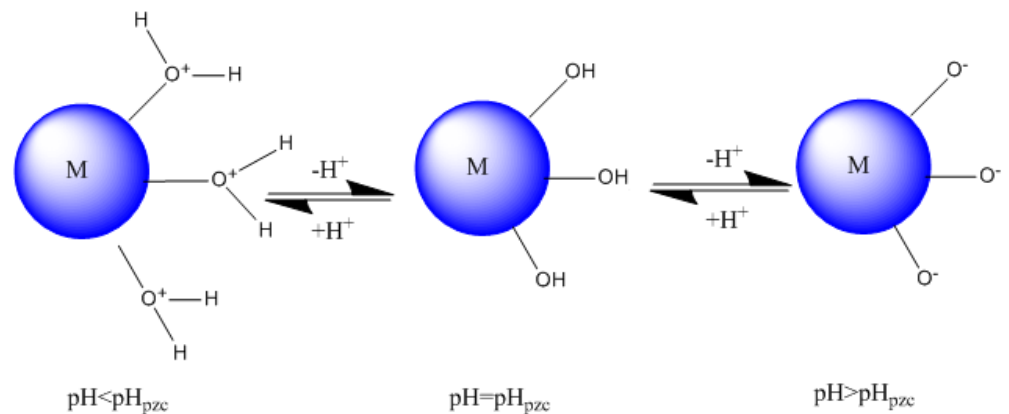


Figure 11. Change in surface contamination of the composite material (M represents HAp/HPMC composite) as a function of pH.

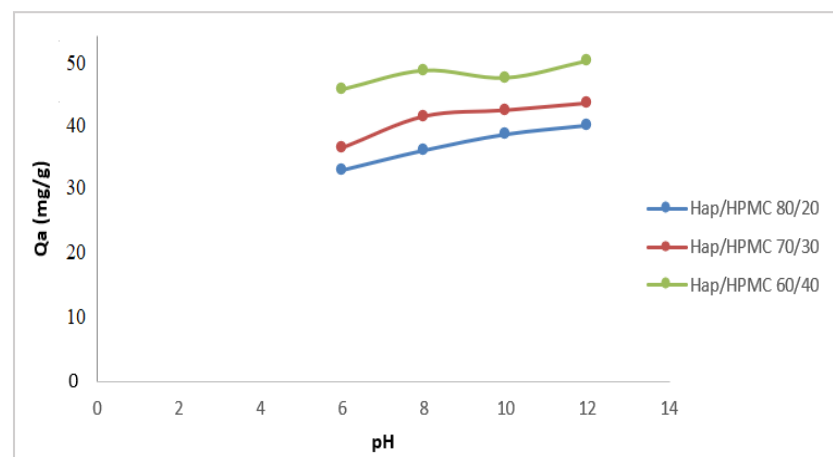


Figure 12. Effect of pH on the adsorption efficacy of the composites, $[\text{MB}] = 53.5 \text{ mg/L}$ and $T = 25 \pm 2 \text{ }^\circ\text{C}$ and $V_{\text{rot}} = 250 \text{ rpm}$.

The adsorption behavior of methylene blue on adsorbents has been studied over a wide pH range from 6 to 12. Adsorption results of MB on the composite show that the maximum adsorption was observed at $\text{pH} = 8$. The increase in the pH value from 6 to 12 was accompanied by a slight increase in the amount of dye adsorbed by HAp/HPMC composites. This behavior may be due to the fact that the surface of the HAp/HPMC composite is negatively contaminated at pH values above pH_{pzc} , which promotes the adsorption of the cationic dye (methylene blue). On the other hand, for pH values below pH_{pzc} , the surface of the HAp/HPMC composite is positively contaminated and, therefore, likely to repel the colorant (the pH_{pzc} of HAp/HPMC is 6.4). As the pH decreases, the number of negatively contaminated sites decreases and the number of positively contaminated sites increases. When the percentage of HPMC increases in the composite, the adsorption increases, indicating an increase in the number of preferential sites for MB adsorption.

By definition, adsorption kinetics represent the progress of the adsorption process of the dye on the adsorbent surface as a function of contact time. It is a very important criterion to consider when evaluating the performance of the selected adsorbent. A good adsorbent must have not only a good adsorption capacity but also a good adsorption rate. The adsorption kinetics of the MB colorant on composites (HAp/HPMC: 80/20, 70/30 and 60/40) were studied by determining the adsorption rate as a function of time while the other variables were kept constant (temperature $25 \text{ }^\circ\text{C}$, pH 8.0, adsorbate mass 53.5 mg (20.0 mL), adsorbent 20 mg, and a mixing speed of 250 rpm). Sample analyses were taken

at regular time intervals to determine the residual concentrations of the MB colorants. The obtained results are shown in Figure 13.

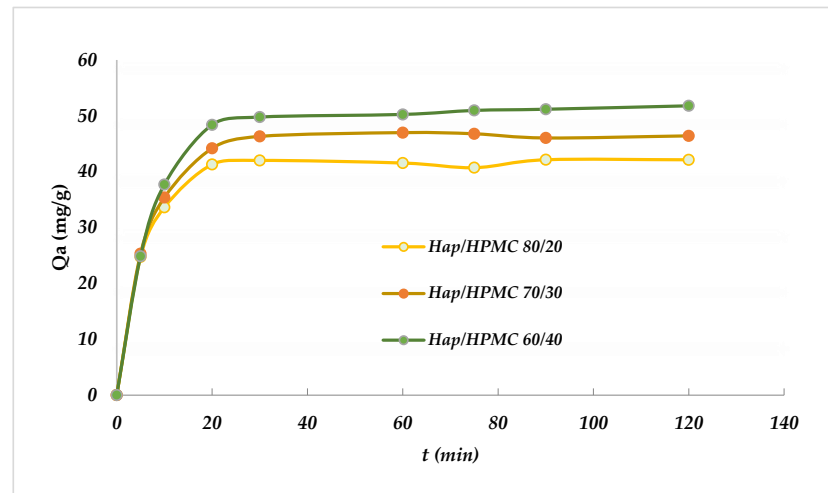


Figure 13. Evolution of the MB adsorbed quantity (Q_a) as a function of time, [MB] = 53.4 mg/L, pH = 7 and $T = 25 \pm 2$ °C, adsorbent 10 mg, $V_{rot} = 250$ rpm.

The results obtained reveal that the quantity of MB bound to the composite increases with time and reaches a maximum adsorption of approximately 51.78 mg/g at 20 min for HAp/HPMC 60/40.

The adsorption at the beginning was rapidly related to the presence of a large number of vacant sites on the surface of the composite used, whereas the slow rate is explained by the decrease in the number of vacant sites and the difficulty of accessing them due to the repulsion forces between MB and the liquid phase.

The effect of initial MB dye concentrations on the adsorption efficiency was evaluated using various initial concentrations ranging from 5 mg/L to 90 mg/L. The adsorption runs were performed at a pH value of 8. The other variables were kept constant, as shown above.

Results are summarized in Figure 14; the results show that the adsorption capacity of the composites increases with the increase in the initial MB concentration, then becomes constant at 40 mg/L. During the adsorption process, MB molecules first reach the surface layer and physically bond to the surface-active sites. Once the surface sites become saturated, the MB molecules diffuse through the surface layer into the porous part of the inner structure of the sorbent. This explains the increase in the rate of adsorption with time.

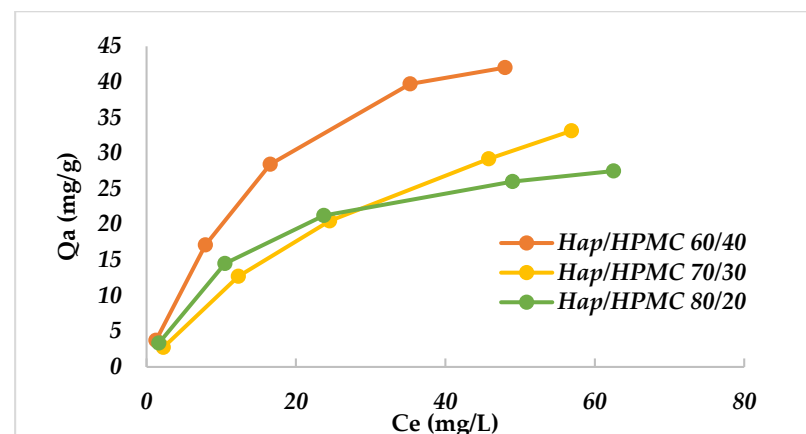


Figure 14. Evolution of the adsorbed quantity as a function of the MB concentration, pH = 7, $T = 25 \pm 2$ °C and $V_{rot} = 250$ rpm.

3.7. Adsorption Isotherms

Adsorption isotherms are commonly used to describe a relationship between the concentration in an aqueous solution and the amount fixed on the adsorbent when the adsorption process reaches equilibrium. The adsorption isotherms were established by contacting aqueous solutions of MB with concentrations ranging between 5 mg/L and 90 mg/L, and 10.0 mg composite, at a pH value of 8 and at room temperature. The Langmuir (Equation (3)) and Freundlich models (Equation (4)) for the adsorption of MB by the composites were examined. Results are summarized in Figures 15 and 16.

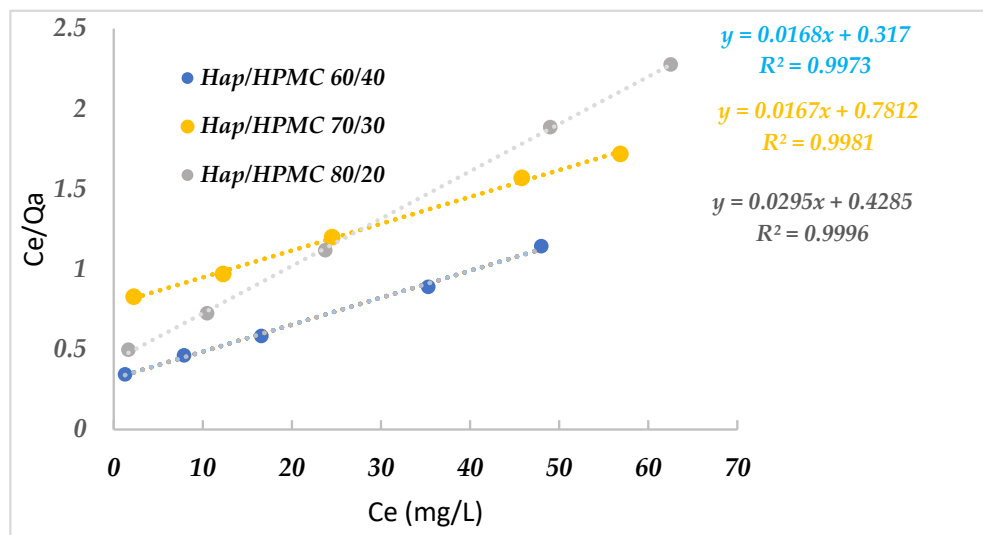


Figure 15. Linearization of the Langmuir equation for the studied adsorbent/adsorbate systems. C_e : concentration of adsorbate, Q_a : adsorbed quantity.

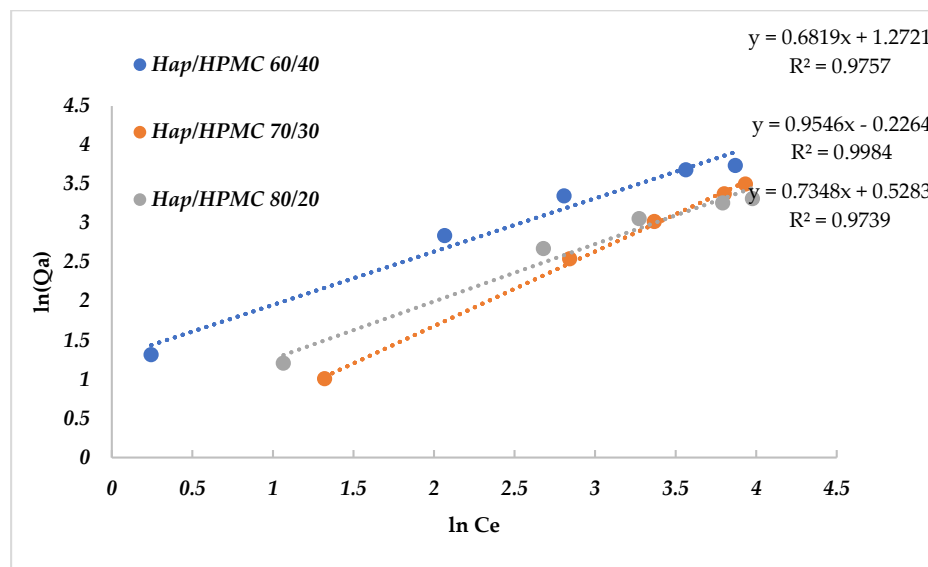


Figure 16. Linearization of the Freundlich equation for adsorbent/adsorbate systems. C_e : concentration of adsorbate, Q_a : adsorbed quantity.

Adsorbent and adsorbate contact time was kept for 2 h under agitation after analysis and determination of the residual concentration. The linear representations of the obtained experimental values of this adsorption process were used to determine the equilibrium parameters and the values of the Langmuir and Freundlich constants calculated by linear regression Tables 3 and 4. The values of the regression coefficients indicate that the adsorp-

tion process of MB by the composites follows the Langmuir isotherm (with excellent linear regression coefficients R^2 , which are very close to one). This implies that the adsorption of MB on the composites occurred in the form of monolayers. The values of Q_{\max} and K_L were obtained from the intercept $C_e/Q_a = f(C_e)$. The maximum adsorption capacities are $59.52 \text{ mg}\cdot\text{g}^{-1}$ for HAp/HPMC 80/20 and $59.88 \text{ mg}\cdot\text{g}^{-1}$ for HAp/HPMC 60/40.

Table 3. Results using the Langmuir model of the MB adsorption isotherm on the HAp/HPMC composite.

Composites	Q_{\max}	K_L	R^2
HAp/HPMC 60/40	59.88	3.89×10^{-2}	0.9996
HAp/HPMC 70/30	53.9	6.88×10^{-2}	0.9981
HAp/HPMC 80/20	59.52	3.920×10^{-2}	0.9973

Table 4. Results using the Freundlich model of the MB adsorption isotherm on the HAp/HPMC composite.

Composites	K_F	n	R^2
HAp/HPMC 60/40	3.568	1.466	0.9757
HAp/HPMC 70/30	0.797	1.048	0.9984
HAp/HPMC 80/20	1.327	1.361	0.9739

A summary of the adsorption efficiency of various adsorbents toward MB is summarized in Table 5.

Table 5. Comparison of adsorption capacities of various adsorbents for MB removal.

Adsorbent	Q_m (mg/g)	pH	Temperature (K)	References
Fly ash	3.07	7.5	303	[80]
Posidonia oceanica	5.56	10	303	[81]
Ulva lactuca	10.99	10	298	[82]
Neem leaf powder	8.76	-	300	[83]
Natural phosphate	7.23	-	298	[84]
Coir pith carbon	5.87	6.9	308	[85]
Clay	6.3	-	293	[86]
Ordered mesoporous silica	54.0	-	295	[87]
Poorly crystalline HAp	14.27	9.0	283	[88]
Natural zeolite	16.37	-	-	[89]
Kaolinite	13.99	-	300	[90]
Sawdust	11.8	7.0	299	[91]
Phosphoric acid modified E	31.15	-	-	[92]
α -chitin nanoparticles	6.90	-	-	[93]
Activated carbon	47.62	-	-	[94]

The values are collected from the published literature. As shown in Table 5, the adsorption efficiency of the 60/40 composite is as good as the ordered mesoporous silica, which shows the highest efficiency [87].

3.8. Adsorption Kinetics

Adsorption kinetics allow estimating the quantity of pollutant adsorbed as a function of time. The kinetics also provide information on the adsorption mechanism and the mode of transfer of the solute from the liquid phase to the solid phase.

Two models have been applied to describe the mechanism of adsorption kinetics, the pseudo-first-order and the pseudo-second-order. Figure 17 shows that $\ln(Q_e - Q_t)$ as a function of time is non-linear. It is deduced that the adsorption kinetics of Methylene Blue on HAp/HPMC cannot be described by pseudo-first-order kinetics. In addition, R^2 values were found to be relatively low. The calculation of Q_e for the different percentages shows that the adsorbed amounts of the MB are rather small compared to the experimental amounts. On the other hand, when comparing the linear representation Figure 18 of t/Q_e

as a function of time, the adsorption capacities at equilibrium and the correlation coefficients calculated for the pseudo-second-order (Table 6) show that this model can describe the kinetic behavior of methylene blue adsorption on the HAp/HPMC composite. Indeed, it was noticed that the correlation coefficients R^2 (pseudo-second-order) are very close to 1, and the values of the adsorption capacities calculated ($Q_{e\text{ cal}}$) from the pseudo-second-order model were very close to the values obtained experimentally ($Q_{e\text{ exp}}$).

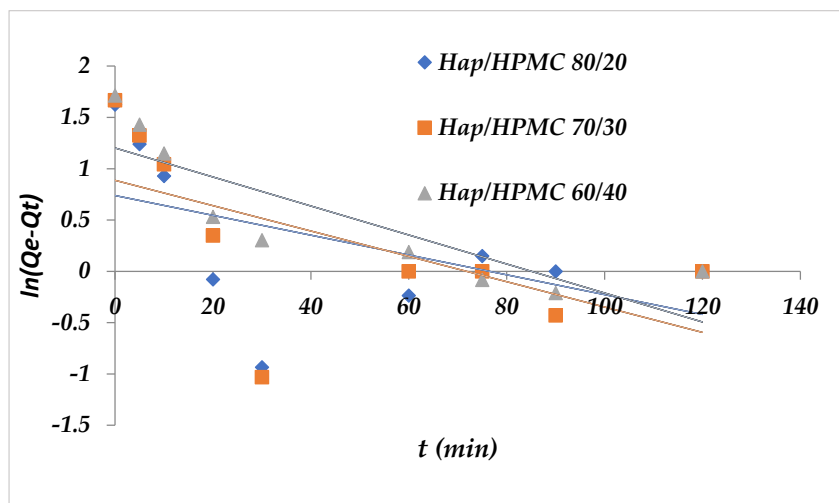


Figure 17. Pseudo-first-order kinetic model applied to the adsorption of MB by the composites.

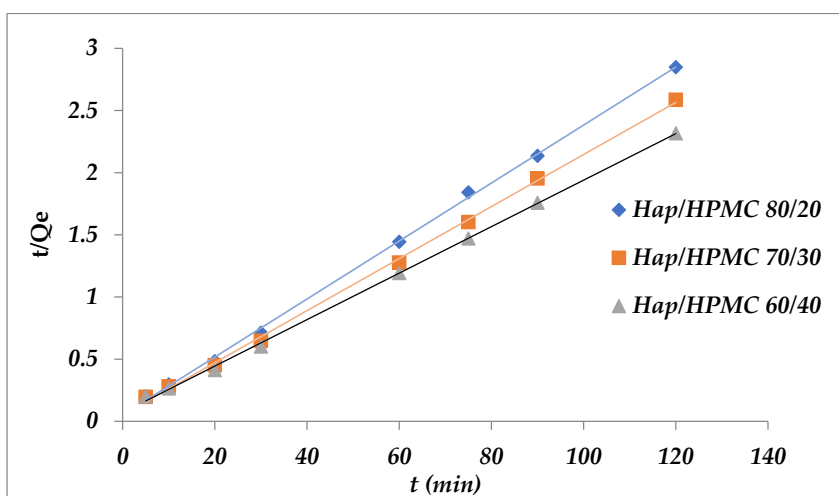


Figure 18. Pseudo-second-order kinetic model applied to the adsorption of MB by the composites.

Table 6. Kinetic parameters of MB adsorption on composites.

Composites	Pseudo-First-Order			Pseudo-Second-Order			
	Q_e	K_1	R^2	$Q_{e\text{ cal}}$	$Q_{e\text{ exp}}$	K_2	R^2
HAp/HPMC 60/40	3.32	0.014	0.728	53.47	51.78	0.005	0.9992
HAp/HPMC 70/30	2.43	0.012	0.365	47.85	46.40	0.008	0.9989
HAp/HPMC 80/20	2.095	0.010	0.260	42.92	42.12	0.011	0.9991

4. Conclusions

In this work, natural-based nanocomposites in the form of membranes were synthesized from HAp and HPMC using the dissolution/re-precipitation method to elaborate nanocomposites. The synthesized composites were characterized by scanning electron microscopy (SEM), calorimetry/thermogravimetric analysis (DSC/TGA), infrared spectroscopy (FT-IR), X-ray photoelectron spectroscopy (XPS), ^{13}C CP/MAS NMR, X-ray fluorescence spectrometry (XRF), and X-ray diffraction (XRD). The composites, as shown by the obtained analysis results, showed a uniform blend with strong interactions between their components. The HAp/HPMC composites were evaluated as adsorbents for the dye synthetic MB form in an aqueous solution. The experimental results showed that the adsorption process can be controlled by various parameters such as solution pH, initial concentration of the dye, and time. The amount of dye adsorbed showed an increase as the pH value increased. It was determined that the zeta potential of the clay increased negatively as the pH increased.

The adsorption kinetics of MB on HAp/HPMC composites shows that the adsorption process is very fast, and equilibrium is established after 20 min. The adsorption mechanism was effectively described by pseudo-second-order kinetics.

Langmuir's model adequately describes the adsorption isotherms of MB on HAp/HPMC composites. The maximum adsorption capacities determined according to the Langmuir isotherm of the composites (HAp/HPMC: 80/20, 60/40) are respectively 59.52 and 59.88 $\text{mg}\cdot\text{g}^{-1}$. These values indicate that the HAp/HPMC 60/40 composite exhibited the best adsorption capacity.

The results of the experiments showed that the dye removal efficiency increases with increasing initial dye concentration.

As a result, it is seen that the removal of cationic dyes, which are an important problem in industrial water treatment, can be achieved by using apatitic composite biomaterials.

Author Contributions: Conceptualization, N.A., K.A. and B.H.; methodology, N.A., K.A., E.M. and B.H.; validation, K.A., L.L.E. and B.H.; writing—original draft preparation, N.A., K.A., M.A., R.S., L.L.E., E.M., B.H. and M.A.-s.; writing—review and editing, L.R., K.A., and M.S.; visualization, M.S.; supervision, K.A., B.H., M.A., R.S. and B.H.; project administration, K.A. and B.H. All authors have read and agreed to the published version of the manuscript.

Funding: The authors have no support or funding to report.

Informed Consent Statement: Not applicable.

Data Availability Statement: The data used to support the findings of this study are available from the corresponding author upon request.

Acknowledgments: Authors would like to thank the department of chemistry at both Mohammed Premier University in Morocco and An-Najah National University in Palestine.

Conflicts of Interest: The authors declare no conflict of interest.

References

1. Rajabi, M.; Mahanpoor, K.; Moradi, O. Removal of dye molecules from aqueous solution by carbon nanotubes and carbon nanotube functional groups: Critical review. *RSC Adv.* **2017**, *7*, 47083–47090. [[CrossRef](#)]
2. Mathur, N. Assessing mutagenicity of textile dyes from pali (rajasthan) using ames bioassay. *Appl. Ecol. Environ. Res.* **2006**, *4*, 111–118. [[CrossRef](#)]
3. Ai, L.; Jiang, J. Removal of methylene blue from aqueous solution with self-assembled cylindrical graphene–carbon nanotube hybrid. *Chem. Eng. J.* **2012**, *192*, 156–163. [[CrossRef](#)]
4. Kacha, S.; Ouali, M.; Elmaleh, S. Dye abatement of textile industry wastewater with bentonite and aluminium salts [flocculation, polyhydroxyaluminium]. *Rev. Des Sci. De L'eau* **1997**, *10*, 233–247.
5. Gücek, A.; Şener, S.; Bilgen, S.; Mazmanlı, M.A. Adsorption and kinetic studies of cationic and anionic dyes on pyrophyllite from aqueous solutions. *J. Colloid Interface Sci.* **2005**, *286*, 53–60. [[CrossRef](#)]
6. Shin, H.-S.; Lee, J.-K. Performance evaluation of electrocoagulation and electrodewatering system for reduction of water content in sewage sludge. *Korean J. Chem. Eng.* **2006**, *23*, 188–193. [[CrossRef](#)]

7. Bhatnagar, A.; Sillanpää, M. Utilization of agro-industrial and municipal waste materials as potential adsorbents for water treatment—A review. *Chem. Eng. J.* **2010**, *157*, 277–296. [[CrossRef](#)]
8. Batzias, F.; Sidiras, D. Dye adsorption by prehydrolysed beech sawdust in batch and fixed-bed systems. *Bioresour. Technol.* **2007**, *98*, 1208–1217. [[CrossRef](#)]
9. Zhang, F.; Zhao, Z.; Tan, R.; Guo, Y.; Cao, L.; Chen, L.; Li, J.; Xu, W.; Yang, Y.; Song, W. Selective and effective adsorption of methyl blue by barium phosphate nano-flake. *J. Colloid Interface Sci.* **2012**, *386*, 277–284. [[CrossRef](#)]
10. Ramírez-Aparicio, J.; Samaniego-Benítez, J.E.; Murillo-Tovar, M.A.; Benítez-Benítez, J.L.; Muñoz-Sandoval, E.; García-Betancourt, M.L. Removal and surface photocatalytic degradation of methylene blue on carbon nanostructures. *Diam. Relat. Mater.* **2021**, *119*, 108544. [[CrossRef](#)]
11. Patel, H.; Vashi, R.T. Treatment of Textile Wastewater by Adsorption and Coagulation. *E-Journal Chem.* **2010**, *7*, 1468–1476. [[CrossRef](#)]
12. Mishra, A.K.; Arockiadoss, T.; Ramaprabhu, S. Study of removal of azo dye by functionalized multi walled carbon nanotubes. *Chem. Eng. J.* **2010**, *162*, 1026–1034. [[CrossRef](#)]
13. Lu, H.-L.; Lee, Y.-H.; Huang, S.-T.; Su, C.; Yang, T.C.-K. Influences of water in bis-benzimidazole-derivative electrolyte additives to the degradation of the dye-sensitized solar cells. *Sol. Energy Mater. Sol. Cells* **2011**, *95*, 158–162. [[CrossRef](#)]
14. Khatibi, E.S.; Haghighi, M.; Mahboob, S. Efficient surface design of reduced graphene oxide, carbon nanotube and carbon active with copper nanocrystals for enhanced simulated-solar-light photocatalytic degradation of acid orange in water. *Appl. Surf. Sci.* **2019**, *465*, 937–949. [[CrossRef](#)]
15. Yang, S.; Wang, L.; Zhang, X.; Yang, W.; Song, G. Enhanced adsorption of Congo red dye by functionalized carbon nanotube/mixed metal oxides nanocomposites derived from layered double hydroxide precursor. *Chem. Eng. J.* **2015**, *275*, 315–321. [[CrossRef](#)]
16. Yang, L.; Luo, Y.; Yang, L.; Luo, S.; Luo, X.; Dai, W.; Li, T.; Luo, Y. Enhanced photocatalytic activity of hierarchical titanium dioxide microspheres with combining carbon nanotubes as “e-bridge”. *J. Hazard. Mater.* **2019**, *367*, 550–558. [[CrossRef](#)]
17. Haji, A.; Shoushtari, A.M.; Abdouss, M. Plasma activation and acrylic acid grafting on polypropylene nonwoven surface for the removal of cationic dye from aqueous media. *Desalination Water Treat.* **2015**, *53*, 3632–3640. [[CrossRef](#)]
18. Haji, A.; Mehrizi, M.K.; Sarani, M. Surface modification of Polypropylene Nonwoven by plasma and β -Cyclodextrin: Optimization and Cationic Dye Removal Studies. *Surf. Interfaces* **2021**, *25*, 101278. [[CrossRef](#)]
19. Goel, N.K.; Kumar, V.; Misra, N.; Varshney, L. Cellulose based cationic adsorbent fabricated via radiation grafting process for treatment of dyes waste water. *Carbohydr. Polym.* **2015**, *132*, 444–451. [[CrossRef](#)]
20. Paulino, A.G.; da Cunha, A.J.; da Silva Alfaya, R.V.; da Silva Alfaya, A.A. Chemically modified natural cotton fiber: A low-cost biosorbent for the removal of the Cu (II), Zn (II), Cd (II), and Pb (II) from natural water. *Desalination Water Treat.* **2014**, *52*, 4223–4233. [[CrossRef](#)]
21. Sun, X.; Yang, L.; Li, Q.; Zhao, J.; Li, X.; Wang, X.; Liu, H. Amino-functionalized magnetic cellulose nanocomposite as adsorbent for removal of Cr(VI): Synthesis and adsorption studies. *Chem. Eng. J.* **2014**, *241*, 175–183. [[CrossRef](#)]
22. Miao, C.; Hamad, W.Y. Cellulose reinforced polymer composites and nanocomposites: A critical review. *Cellulose* **2013**, *20*, 2221–2262. [[CrossRef](#)]
23. Yue, X.; Huang, J.; Jiang, F.; Lin, H.; Chen, Y. Synthesis and characterization of cellulose-based adsorbent for removal of anionic and cationic dyes. *J. Eng. Fibers Fabr.* **2019**, *14*, 1558925019828194. [[CrossRef](#)]
24. Azzaoui, K.; Mejdoubi, E.; Lamhamdi, A.; Zaoui, S.; Berrabah, M.; Elidrissi, A.; Hammouti, B.; Fouda, M.M.; Al-Deyab, S.S. Structure and properties of hydroxyapatite/hydroxyethyl cellulose acetate composite films. *Carbohydr. Polym.* **2015**, *115*, 170–176. [[CrossRef](#)] [[PubMed](#)]
25. Hamed, O.; Abu Lail, B.; Deghles, A.; Qasem, B.; Azzaoui, K.; Abu Obied, A.; Algarra, M.; Jodeh, S. Synthesis of a cross-linked cellulose-based amine polymer and its application in wastewater purification. *Environ. Sci. Pollut. Res.* **2019**, *26*, 28080–28091. [[CrossRef](#)]
26. Tan, I.A.W.; Hameed, B.H.; Ahmad, A.L. Equilibrium and kinetic studies on basic dye adsorption by oil palm fibre activated carbon. *Chem. Eng. J.* **2007**, *127*, 111–119. [[CrossRef](#)]
27. Juang, R.-S.; Wu, F.C.; Tseng, R.L. The Ability of Activated Clay for the Adsorption of Dyes from Aqueous Solutions. *Environ. Technol.* **1997**, *18*, 525–531. [[CrossRef](#)]
28. Aadil, K.R.; Barapatre, A.; Jha, H. Synthesis and characterization of Acacia lignin-gelatin film for its possible application in food packaging. *Bioresour. Bioprocess.* **2016**, *3*, 220. [[CrossRef](#)]
29. Lamhamdi, A.; Azzaoui, K.; Mejdoubi, E.; Garoiz, H.; Berabah, M.; Elbali, B.; Hammouti, B. Contribution of adsorption of metals using calcium phosphates in the presence of support polyethylene glycol. *Mor. J. Chem.* **2014**, *2*, 90–96.
30. Akartasse, N.; Mejdoubi, E.; Razzouki, B.; Azzaoui, K.; Jodeh, S.; Hamed, O.; Ramdani, M.; Lamhamdi, A.; Berrabah, M.; Lahmass, I.; et al. Natural product based composite for extraction of arsenic (III) from waste water. *Chem. Central J.* **2017**, *11*, 33. [[CrossRef](#)]
31. Elyahyaoui, A.; Ellouzi, K.; Al Zabadi, H.; Razzouki, B.; Bouhlassa, S.; Azzaoui, K.; Mejdoubi, E.M.; Hamed, O.; Jodeh, S.; Lamhamdi, A. Adsorption of Chromium (VI) on Calcium Phosphate: Mechanisms and Stability Constants of Surface Complexes. *Appl. Sci.* **2017**, *7*, 222. [[CrossRef](#)]
32. Razzouki, B.; El Hajjaji, S.; Azzaoui, K.; Errich, A.; Lamhamdi, A.; Berrabah, M.; Elansari, L.L. Physicochemical study of arsenic removal using iron hydroxide. *J. Mater. Environ. Sci.* **2015**, *6*, 144–1450.

33. Fallah, S.; Mamaghani, H.R.; Yegani, R.; Hajinajaf, N.; Pourabbas, B. Use of graphene substrates for wastewater treatment of textile industries. *Adv. Compos. Hybrid Mater.* **2020**, *3*, 187–193. [[CrossRef](#)]
34. Ayodele, O.; Olusegun, S.J.; Oluwasina, O.O.; Okoronkwo, E.A.; Olanipekun, E.O.; Mohallem, N.D.; Guimarães, W.G.; Gomes, B.L.d.M.; Souza, G.d.O.; Duarte, H.A. Experimental and theoretical studies of the adsorption of Cu and Ni ions from wastewater by hydroxyapatite derived from eggshells. *Environ. Nanotechnol. Monit. Manag.* **2021**, *15*, 100439. [[CrossRef](#)]
35. Roszkopfová, O.; Galamboš, M.; Pivarčiová, L.; Čaplovičová, M.; Rajec, P. Adsorption of nickel on synthetic hydroxyapatite from aqueous solutions. *J. Radioanal. Nucl. Chem. Artic.* **2013**, *295*, 459–465. [[CrossRef](#)]
36. Chen, S.B.; Ma, Y.B.; Chen, L.; Xian, K. Adsorption of aqueous Cd²⁺, Pb²⁺, Cu²⁺ ions by nano-hydroxyapatite: Single- and multi-metal competitive adsorption study. *Geochem. J.* **2010**, *44*, 233–239. [[CrossRef](#)]
37. Feng, Y.; Gong, J.-L.; Zeng, G.-M.; Niu, Q.-Y.; Zhang, H.-Y.; Niu, C.-G.; Deng, J.-H.; Yan, M. Adsorption of Cd (II) and Zn (II) from aqueous solutions using magnetic hydroxyapatite nanoparticles as adsorbents. *Chem. Eng. J.* **2010**, *162*, 487–494. [[CrossRef](#)]
38. Zou, X.; Zhao, Y.; Zhang, Z. Preparation of hydroxyapatite nanostructures with different morphologies and adsorption behavior on seven heavy metals ions. *J. Contam. Hydrol.* **2019**, *226*, 103538. [[CrossRef](#)]
39. Jiang, J.; Long, Y.; Hu, X.; Hu, J.; Zhu, M.; Zhou, S. A facile microwave-assisted synthesis of mesoporous hydroxyapatite as an efficient adsorbent for Pb²⁺ adsorption. *J. Solid State Chem.* **2020**, *289*, 121491. [[CrossRef](#)]
40. El-Nagar, D.A.; Massoud, S.A.; Ismail, S.H. Removal of some heavy metals and fungicides from aqueous solutions using nano-hydroxyapatite, nano-bentonite and nanocomposite. *Arab. J. Chem.* **2020**, *13*, 7695–7706. [[CrossRef](#)]
41. Ahmadi, S.A.R.; Kalaei, M.R.; Moradi, O.; Nosratinia, F.; Abdouss, M. Core-shell activated carbon-ZIF-8 nanomaterials for the removal of tetracycline from polluted aqueous solution. *Adv. Compos. Hybrid Mater.* **2021**, *4*, 1384–1397. [[CrossRef](#)]
42. Deng, Z.; Sun, S.; Li, H.; Pan, D.; Patil, R.R.; Guo, Z.; Seok, I. Modification of coconut shell-based activated carbon and purification of wastewater. *Adv. Compos. Hybrid Mater.* **2021**, *4*, 65–73. [[CrossRef](#)]
43. Saleh, T.; Sari, A.; Tuzen, M. Effective adsorption of antimony(III) from aqueous solutions by polyamide-graphene composite as a novel adsorbent. *Chem. Eng. J.* **2017**, *307*, 230–238. [[CrossRef](#)]
44. Ishikawa, T.; Tanaka, H.; Yasukawa, A.; Kandori, K. Modification of calcium hydroxyapatite using ethyl phosphates. *J. Mater. Chem.* **1995**, *5*, 1963–1967. [[CrossRef](#)]
45. Zakharov, N.A.; Ezhova, Z.A.; Koval', E.M.; Kalinnikov, V.T.; Chalykh, A. Hydroxyapatite-Carboxymethyl Cellulose Nanocomposite Biomaterial. *Inorg. Mater.* **2005**, *41*, 509–515. [[CrossRef](#)]
46. Wahl, D.; Czernuszka, J. Collagen-Hydroxyapatite Composites for Hard Tissue Repair. *Eur. Cells Mater.* **2006**, *11*, 43–56. [[CrossRef](#)]
47. Lickorish, D.; Ramshaw, J.A.; Werkmeister, J.A.; Glattauer, V.; Howlett, C.R. Collagen-hydroxyapatite composite prepared by biomimetic process. *J. Biomed. Mater. Res. Part A Off. J. Soc. Biomater. Jpn. Soc. Biomater. Aust. Soc. Biomater. Korean Soc. Biomater.* **2004**, *68*, 19–27. [[CrossRef](#)]
48. Teng, S.-H.; Lee, E.-J.; Wang, P.; Kim, H.-E. Collagen/hydroxyapatite composite nanofibers by electrospinning. *Mater. Lett.* **2008**, *62*, 3055–3058. [[CrossRef](#)]
49. Koupaei, N.; Karkhaneh, A. Porous crosslinked polycaprolactone hydroxyapatite networks for bone tissue engineering. *Tissue Eng. Regen. Med.* **2016**, *13*, 251–260. [[CrossRef](#)]
50. Ritzoulis, C.; Scoutaris, N.; Demetriou, E.; Papademetriou, K.; Kokkou, S.; Stavroulias, S.; Panayiotou, C. Formation of hydroxyapatite/biopolymer biomaterials. I. Microporous composites from solidified emulsions. *J. Biomed. Mater. Res. Part A Off. J. Soc. Biomater. Jpn. Soc. Biomater. Aust. Soc. Biomater. Korean Soc. Biomater.* **2004**, *71*, 675–684. [[CrossRef](#)]
51. Senthilarasan, K.; Ragu, A.; Sakthivel, P. Synthesis and characterization of nano hydroxyapatite with agar-agar bio-polymer. *Int. J. Eng. Res. Appl.* **2014**, *4*, 55–59.
52. Yoshida, A.; Miyazaki, T.; Ishida, E.; Ashizuka, M. Preparation of Bioactive Chitosan-hydroxyapatite Nanocomposites for Bone Repair through Mechanochemical Reaction. *Mater. Trans.* **2004**, *45*, 994–998. [[CrossRef](#)]
53. Zhang, J.; Wang, Q.; Wang, A. In situ generation of sodium alginate/hydroxyapatite nanocomposite beads as drug-controlled release matrices. *Acta Biomater.* **2010**, *6*, 445–454. [[CrossRef](#)] [[PubMed](#)]
54. Hossan, M.; Gafur, M.; Karim, M.; Rana, A. Mechanical properties of Gelatin-Hydroxyapatite composite for bone tissue engineering. *Bangladesh J. Sci. Ind. Res.* **2015**, *50*, 15–20. [[CrossRef](#)]
55. Chen, S.; Du, X.; Wang, T.; Jia, L.; Huang, D.; Chen, W. Synthesis of near-infrared responsive gold nanorod-doped gelatin/hydroxyapatite composite microspheres with controlled photo-thermal property. *Ceram. Int.* **2018**, *44*, 900–904. [[CrossRef](#)]
56. Tavakol, S.; Nikpour, M.R.; Amani, A.; Soltani, M.; Rabiee, S.M.; Rezayat, S.M.; Chen, P.; Jahanshahi, M. Bone regeneration based on nano-hydroxyapatite and hydroxyapatite/chitosan nanocomposites: An in vitro and in vivo comparative study. *J. Nanoparticle Res.* **2013**, *15*, 1373. [[CrossRef](#)]
57. Nikpour, M.; Rabiee, S.; Jahanshahi, M. Synthesis and characterization of hydroxyapatite/chitosan nanocomposite materials for medical engineering applications. *Compos. Part B Eng.* **2012**, *43*, 1881–1886. [[CrossRef](#)]
58. Vila, M.; Sánchez-Salcedo, S.; Cicuéndez, M.; Izquierdo-Barba, I.; Vallet-Regí, M. Novel biopolymer-coated hydroxyapatite foams for removing heavy-metals from polluted water. *J. Hazard. Mater.* **2011**, *192*, 71–77. [[CrossRef](#)]
59. Williams, D.; European Society for Biomaterials. *Definitions in Biomaterials: Proceedings of a Consensus Conference of the European Society for Biomaterials, Chester, UK, 3–5 March 1986*; Elsevier: Amsterdam, The Netherlands; New York, NY, USA, 1987.

60. Mejdoubi, E.; Azzaoui, A.L.; Berrabah, M.K.; Akartasse, N. *Elaboration De Nouvelles Membranes Spongieuses Et Denses, a Base De Nanoparticules Apatitiques, Destinees Aux Usages Orthopediques Et Odontologiques*; Office Marocain De La Propriété Industrielle Et Commerciale OMPIC, O. University Mohammed 1st: Oujda, Morocco, 2020; p. 17.
61. Azzaoui, K.; Mejdoubi, E.; Lamhamdi, A.; Jodeh, S.; Hamed, O.; Berrabah, M.; Jerdioui, S.; Salghi, R.; Akartasse, N.; Errich, A.; et al. Preparation and characterization of biodegradable nanocomposites derived from carboxymethyl cellulose and hydroxyapatite. *Carbohydr. Polym.* **2017**, *167*, 59–69. [[CrossRef](#)]
62. El-Bahy, S.M.; El-Bahy, Z.M. Synthesis and characterization of polyamidoxime chelating resin for adsorption of Cu (II), Mn (II) and Ni (II) by batch and column study. *J. Environ. Chem. Eng.* **2016**, *4*, 276–286. [[CrossRef](#)]
63. Huang, X.; Pan, M. RETRACTED: The highly efficient adsorption of Pb(II) on graphene oxides: A process combined by batch experiments and modeling techniques. *J. Mol. Liq.* **2016**, *215*, 410–416. [[CrossRef](#)]
64. Nazari, G.; Abolghasemi, H.; Esmaili, M. Batch adsorption of cephalexin antibiotic from aqueous solution by walnut shell-based activated carbon. *J. Taiwan Inst. Chem. Eng.* **2016**, *58*, 357–365. [[CrossRef](#)]
65. Gerente, C.; Lee, V.K.C.; Le Cloirec, P.; McKay, G. Application of Chitosan for the Removal of Metals from Wastewaters by Adsorption—Mechanisms and Models Review. *Crit. Rev. Environ. Sci. Technol.* **2007**, *37*, 41–127. [[CrossRef](#)]
66. Subhashree, S.; Chakraborti, C.K.; Mishra, S.C.; Naik, S. Qualitative analysis of controlled release ofloxacin/HPMC mucoadhesive suspension. *Int. J. Drug Dev. Res.* **2011**, *3*.
67. Pawar, H.V.; Tetteh, J.; Boateng, J.S. Preparation, optimisation and characterisation of novel wound healing film dressings loaded with streptomycin and diclofenac. *Colloids Surf. B Biointerfaces* **2013**, *102*, 102–110. [[CrossRef](#)]
68. Caykara, T.; Demirci, S.; Eroğlu, M.S.; Güven, O. Poly(ethylene oxide) and its blends with sodium alginate. *Polymer* **2005**, *46*, 10750–10757. [[CrossRef](#)]
69. Kergourlay, E. Apatites Nanocristallines Biomimétiques Carbonatées Pour Applications Médicales: De La Synthèse Des Poudres Aux Revêtements Par Projection Dynamique à Froid (Cold Spray). 2016. Available online: <https://oatao.univ-toulouse.fr/25381/> (accessed on 1 April 2022).
70. Alexander, L. X-ray diffraction methods in polymer science. *J. Mater. Sci.* **1971**, *6*, 93. [[CrossRef](#)]
71. Xianmiao, C.; Yubao, L.; Yi, Z.; Li, Z.; Jidong, L.; Huanan, W. Properties and in vitro biological evaluation of nano-hydroxyapatite/chitosan membranes for bone guided regeneration. *Mater. Sci. Eng. C* **2009**, *29*, 29–35. [[CrossRef](#)]
72. Bigi, A.; Cojazzi, G.; Panzavolta, S.; Ripamonti, A.; Roveri, N.; Romanello, M.; Suarez, K.N.; Moro, L. Chemical and structural characterization of the mineral phase from cortical and trabecular bone. *J. Inorg. Biochem.* **1997**, *68*, 45–51. [[CrossRef](#)]
73. Weng, L.; Poleunis, C.; Bertrand, P.; Carlier, V.; Sclavons, M.; Franquinet, P.; Legras, R. Sizing removal and functionalization of the carbon fiber surface studied by combined TOF SIMS and XPS. *J. Adhes. Sci. Technol.* **1995**, *9*, 859–871. [[CrossRef](#)]
74. Kolmas, J.; Piotrowska, U.; Kuras, M.; Kurek, E. Effect of carbonate substitution on physicochemical and biological properties of silver containing hydroxyapatites. *Mater. Sci. Eng. C* **2017**, *74*, 124–130. [[CrossRef](#)] [[PubMed](#)]
75. Lopez-Ramon, M.V.; Stoeckli, F.; Moreno-Castilla, C.; Carrasco-Marin, F. On the characterization of acidic and basic surface sites on carbons by various techniques. *Carbon* **1999**, *37*, 1215–1221. [[CrossRef](#)]
76. Kragović, M.; Stojmenović, M.; Petrović, J.; Loredó, J.; Pašalić, S.; Nedeljković, A.; Ristović, I. Influence of Alginate Encapsulation on Point of Zero Charge (pHpzc) and Thermodynamic Properties of the Natural and Fe(III)—Modified Zeolite. *Procedia Manuf.* **2019**, *32*, 286–293. [[CrossRef](#)]
77. Tanaka, H.; Watanabe, T.; Chikazawa, A.M. FTIR and TPD studies on the adsorption of pyridine, n-butylamine and acetic acid on calcium hydroxyapatite. *J. Chem. Soc. Faraday Trans.* **1997**, *93*, 4377–4381. [[CrossRef](#)]
78. Markovic, M.; Fowler, B.O.; Tung, M.S. Preparation and comprehensive characterization of a calcium hydroxyapatite reference material. *J. Res. Natl. Inst. Stand. Technol.* **2004**, *109*, 553–568. [[CrossRef](#)]
79. Crini, G.; Badot, P.-M. Application of chitosan, a natural aminopolysaccharide, for dye removal from aqueous solutions by adsorption processes using batch studies: A review of recent literature. *Prog. Polym. Sci.* **2008**, *33*, 399–447. [[CrossRef](#)]
80. Rao, V.B.; Rao, S.R.M. Adsorption studies on treatment of textile dyeing industrial effluent by flyash. *Chem. Eng. J.* **2006**, *116*, 77–84.
81. Ncibi, M.C.; Mahjoub, B.; Seffen, M. Kinetic and equilibrium studies of methylene blue biosorption by *Posidonia oceanica* (L.) fibres. *J. Hazard. Mater.* **2007**, *139*, 280–285. [[CrossRef](#)]
82. El Sikaily, A.; Khaled, A.; El Nemr, A.; Abdelwahab, O. Removal of Methylene Blue from aqueous solution by marine green alga *Ulva lactuca*. *Chem. Ecol.* **2006**, *22*, 149–157. [[CrossRef](#)]
83. Bhattacharyya, K.; Sharma, A. Kinetics and thermodynamics of Methylene Blue adsorption on Neem (*Azadirachta indica*) leaf powder. *Dye. Pigment.* **2005**, *65*, 51–59. [[CrossRef](#)]
84. Barka, N.; Assabbane, A.; Nounah, A.; Laanab, L.; Ichou, Y.A. Removal of textile dyes from aqueous solutions by natural phosphate as a new adsorbent. *Desalination* **2009**, *235*, 264–275. [[CrossRef](#)]
85. Kavitha, D.; Namasivayam, C. Experimental and kinetic studies on methylene blue adsorption by coir pith carbon. *Bioresour. Technol.* **2007**, *98*, 14–21. [[CrossRef](#)] [[PubMed](#)]
86. Gürses, A.; Karaca, S.; Doğar, Ç.; Bayrak, R.; Açıkyıldız, M.; Yalçın, M. Determination of adsorptive properties of clay/water system: Methylene blue sorption. *J. Colloid Interface Sci.* **2004**, *269*, 310–314. [[CrossRef](#)] [[PubMed](#)]
87. Ho, K.Y.; McKay, G.; Yeung, K.L. Selective Adsorbents from Ordered Mesoporous Silica. *Langmuir* **2003**, *19*, 3019–3024. [[CrossRef](#)]
88. Wei, W.; Yang, L.; Zhong, W.H.; Li, S.Y.; Cui, J.; Wei, Z.G. Fast removal of methylene blue from aqueous solution by adsorption onto poorly crystalline hydroxyapatite nanoparticles. *Dig. J. Nanomater. Biostruct.* **2015**, *19*, 1343–1363.

89. Han, R.; Zhang, J.; Han, P.; Wang, Y.; Zhao, Z.; Tang, M. Study of equilibrium, kinetic and thermodynamic parameters about methylene blue adsorption onto natural zeolite. *Chem. Eng. J.* **2009**, *145*, 496–504. [[CrossRef](#)]
90. Ghosh, D.; Bhattacharyya, K.G. Adsorption of methylene blue on kaolinite. *Appl. Clay Sci.* **2002**, *20*, 295–300. [[CrossRef](#)]
91. Hamdaoui, O. Batch study of liquid-phase adsorption of methylene blue using cedar sawdust and crushed brick. *J. Hazard. Mater.* **2006**, *135*, 264–273. [[CrossRef](#)]
92. Agarwal, S.; Tyagi, I.; Gupta, V.K.; Ghasemi, N.; Shahivand, M.; Ghasemi, M. Kinetics, equilibrium studies and thermodynamics of methylene blue adsorption on Ephedra strobilacea saw dust and modified using phosphoric acid and zinc chloride. *J. Mol. Liq.* **2016**, *218*, 208–218. [[CrossRef](#)]
93. Dhananasekaran, S.; Palanivel, R.; Pappu, S. Adsorption of methylene blue, bromophenol blue, and coomassie brilliant blue by α -chitin nanoparticles. *J. Adv. Res.* **2016**, *7*, 113–124. [[CrossRef](#)]
94. Pathania, D.; Sharma, S.; Singh, P. Removal of methylene blue by adsorption onto activated carbon developed from *Ficus carica* bast. *Arab. J. Chem.* **2017**, *10*, S1445–S1451. [[CrossRef](#)]